Modeling of Mars' ionospheric electrodynamics under various local magnetic field topologies

AGU P23A-1909

Jérémy A. Riousset,[1] Carol S. Paty,[1] Robert J. Lillis,[2] Matthew O. Fillingim,[2] Scott L. England,[2] Paul G. Withers,[3] and John P. M. Hale[1]

[1]School of Earth and Atmospheric Sciences, Georgia Tech, Atlanta, GA, 30306, USA (riousset@gatech.edu; carol.paty@eas.gatech.edu)

[2]Space Sciences Lab, UC Berkeley, Berkeley, CA, 94720, USA (rlillis@ssl.berkeley.edu; matt@ssl.berkeley.edu; england@ssl.berkeley.edu)

[3]Astronomy Department, Boston U, Boston, MA, 02215, USA (withers@bu.edu)

Georgia Tech

BOSTON UNIVERSITY

Abstract

The interactions between Mars' unique crustal magnetic fields and upper atmospheric electrons, ions and neutrals lead to the formation of currents in the ionospheric dynamo region. These interactions involve elastic and inelastic collisions between ions, electrons and neutrals in the presence of varying pressures, temperatures and densities. The remanent fields embedded in the crust provide Mars with a very rich magnetic topology with significant variations in terms of geometry and magnitude on the order of a few tens to hundreds of kilometers spatially and several orders of magnitude in amplitude. Here we present mesoscale, three-dimensional, multi-fluid, self-consistent simulations of Mars' ionospheric electrodynamics in the dynamo region (~100–400 km altitude), where differential motion of ions and electrons occurs. Our investigations focus on the influence of the magnetic field strength and geometry, and neutral wind speeds, on the dynamo current. We look in particular at the influence of the magnetic field magnitude through simpler, uniform geometries. In addition, our model is able to simulate highly non-uniform magnetic fields involving cusps and loops. To achieve these geometries, we position a small magnetic dipole in the crust and are able to produce representative field configurations. The work presented here investigates the effects of thermospheric neutral winds and magnetic topologies for the dayside ionosphere on the formation and evolution of ionospheric currents on Mars. These simulation predictions will be compared to the data from Mars Atmosphere and Volatile EvolutioN (MAVEN) mission starting in early 2015. They will ultimately help to assess the ionospheric effects on future missions to the Red Planet.

I. Introduction

The motivations for our model are as follows:

- Ionospheric composition (e & 71% O_2^+, 25% CO_2^+, 4% O^+) ⇒ multifluid model *Paty and Winglee* [2006]
- Neutral winds ⇒ 3-D model
- Complex magnetic field configuration (Figures 1 & 2) ⇒ systematic validation approach
- 100 km×50 km×400 km space scale ⇒ efficient numerical model

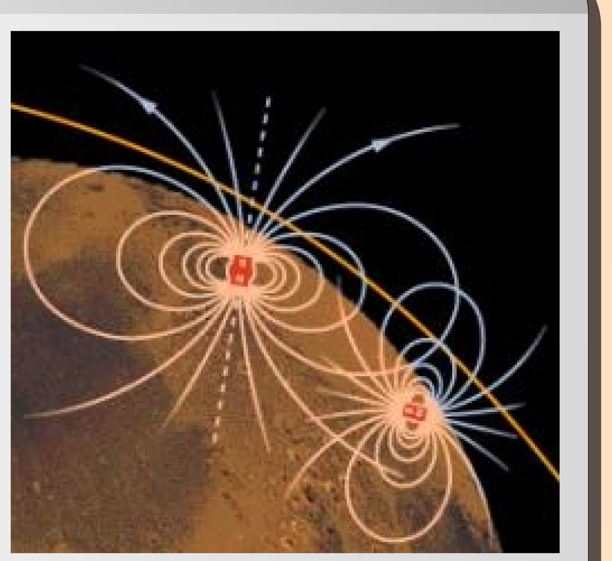

Figure 1: View of Mars' remnant crustal magnetic field. Figure courtesy of Jack Connerney.

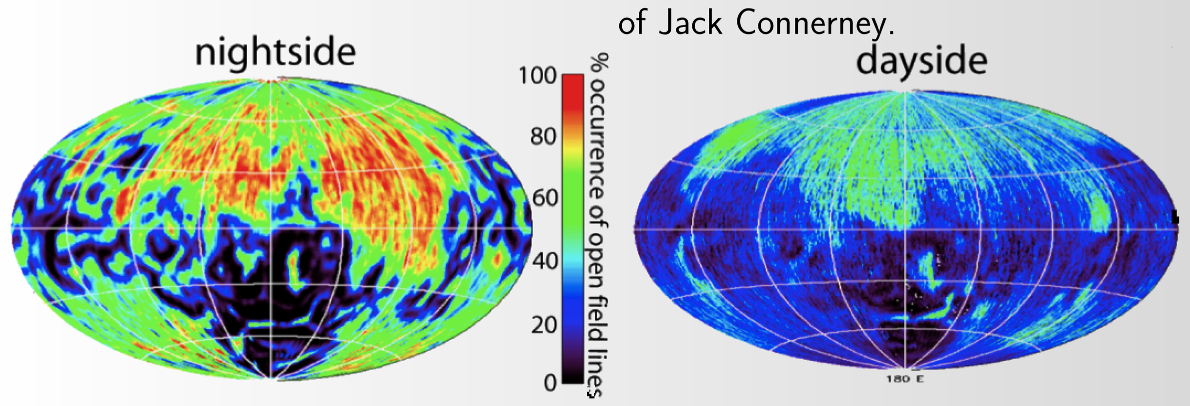

Figure 2: The percent occurrence of open magnetic field lines (i.e. connecting the IMF to the Martian atmosphere) at ~400 km altitude on the nightside and dayside [*Brain et al.*, 2007].

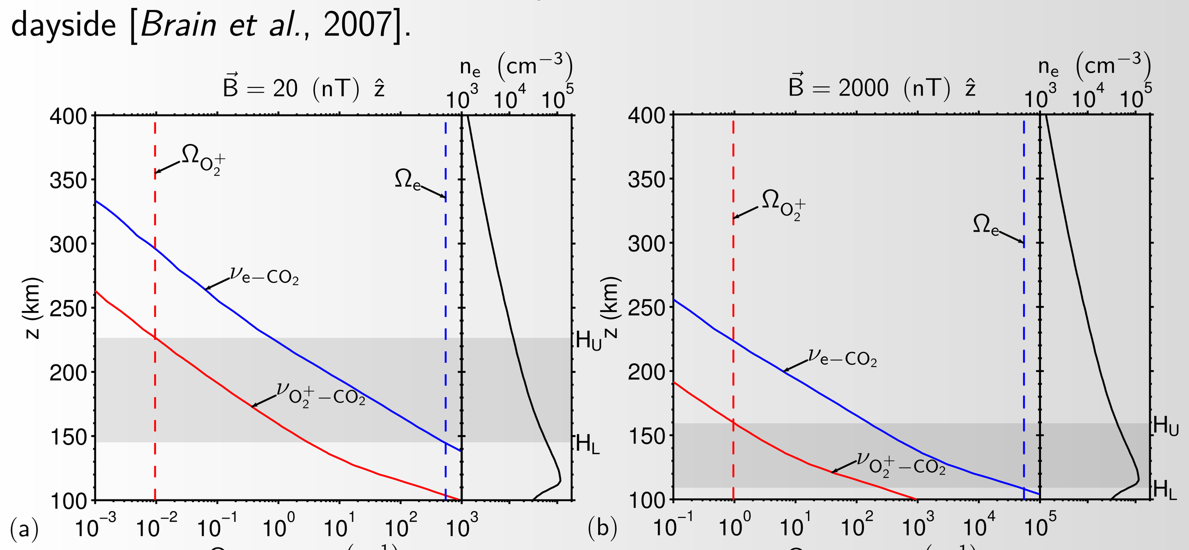

Figure 3: Estimated altitude of the dynamo region for a uniform magnetic field (a) $\vec{B}$=20 nT $\hat{z}$, (b) $\vec{B}$=2000 nT $\hat{z}$

II. Model Formulation

- A 2-step Runge-Kutta method is used [*Balay et al.*, 1997; *Pacheco*, 1996; *Press et al.*, 1992]
- Neumann boundary conditions are employed
- i=O_2^+, CO_2^+, O^+; e=electron

- Fundamental equations
- Elastic ion-neutral collision
- Electron-neutral collisions

$$\frac{\partial P_i}{\partial t} = -\nabla\cdot\left(P_i\vec{V}_i\right) + (\gamma_i - 1)\vec{V}_i\cdot\nabla P_i \quad (1)$$

$$\frac{\partial P_e}{\partial t} = -\nabla\cdot\left(P_e\vec{V}_e\right) + (\gamma_e - 1)\vec{V}_e\cdot\nabla P_e \quad (2)$$

$$\rho_i\frac{\partial \vec{V}_i}{\partial t} = -\rho_i\left(\vec{V}_i\cdot\nabla\right)\vec{V}_i + e\,n_i\left(\vec{E}+\vec{V}_i\times\vec{B}\right) - \nabla P_i + \frac{\rho_i\vec{g}_M}{\left(1+\frac{z}{R_M}\right)^2} + \sum_n \rho_i\nu_{i-n}\left(\vec{V}_n-\vec{V}_i\right) \quad (3)$$

$$\vec{V}_e = \sum_i \frac{n_i\vec{V}_i}{n_e} - \frac{\vec{J}}{e\,n_e} \quad (4)$$

$$\vec{E} = -\vec{V}_e\times\vec{B} - \frac{\nabla P_e}{e\,n_e} + \frac{m_e}{e}\sum_n \nu_{n-e}\left(\vec{V}_n-\vec{V}_e\right) \quad (5)$$

$$\frac{\partial n_i}{\partial t} = -\nabla\cdot\left(n_i\vec{V}_i\right) \quad (6) \qquad n_e = \sum_i n_i \quad (8)$$

$$\frac{\partial \vec{B}}{\partial t} = -\nabla\times\vec{E} \quad (7) \qquad \vec{J} = \frac{\nabla\times\vec{B}}{\mu_0} \quad (9)$$

III. Initial Conditions

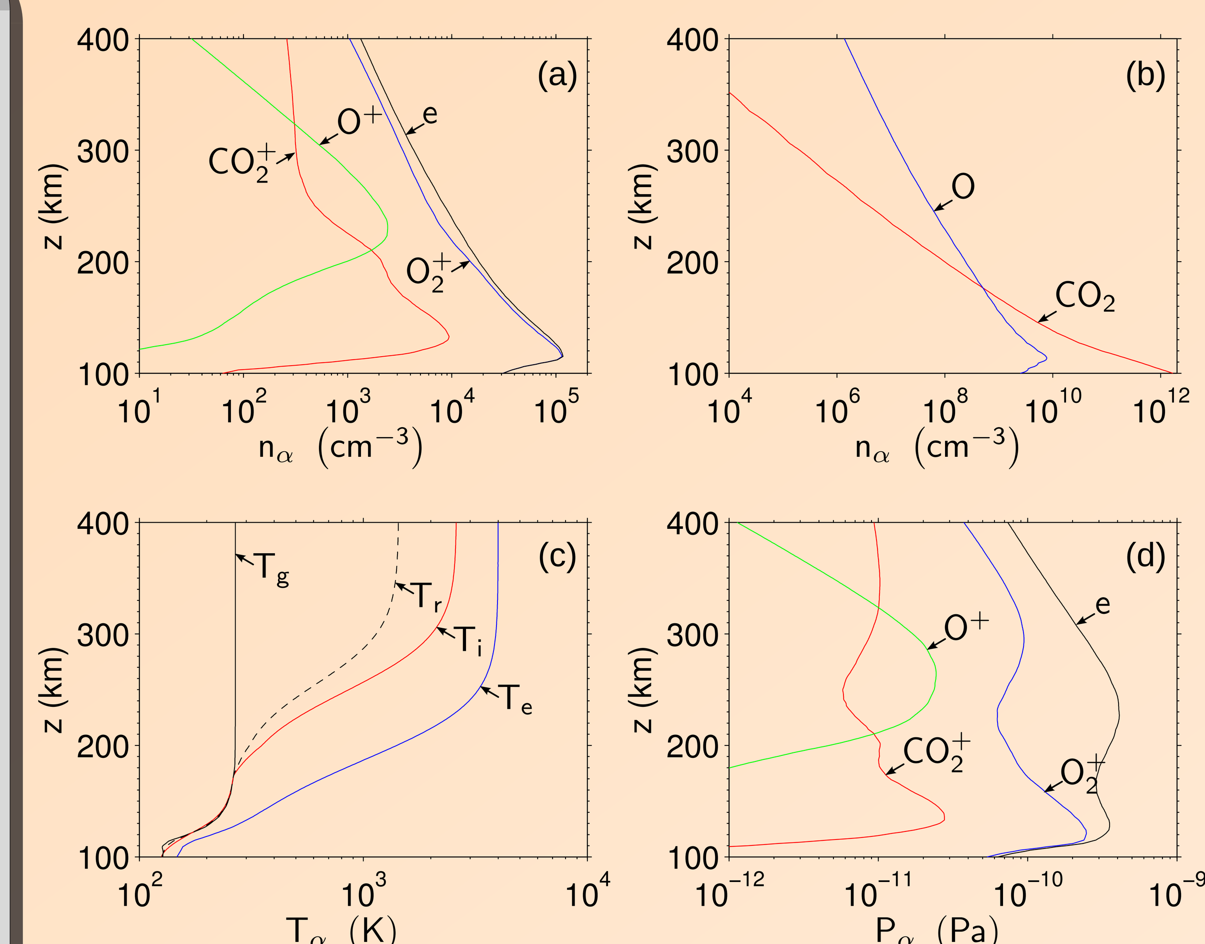

Figure 4: Initial profiles used for the simulation run presented in this paper. The ionization and electron number density profiles are derived from the Mars Climate Database [*Lewis et al.*, 1999] using a photoionization model [*Lillis et al.*, 2012]. The conditions are those of Mars year 24, moderate solar condition, 0° latitude, 0° longitude, Northern autumnal equinox (L_s=180°) for 2 PM local time.

IV. Uniform Vertical Fields

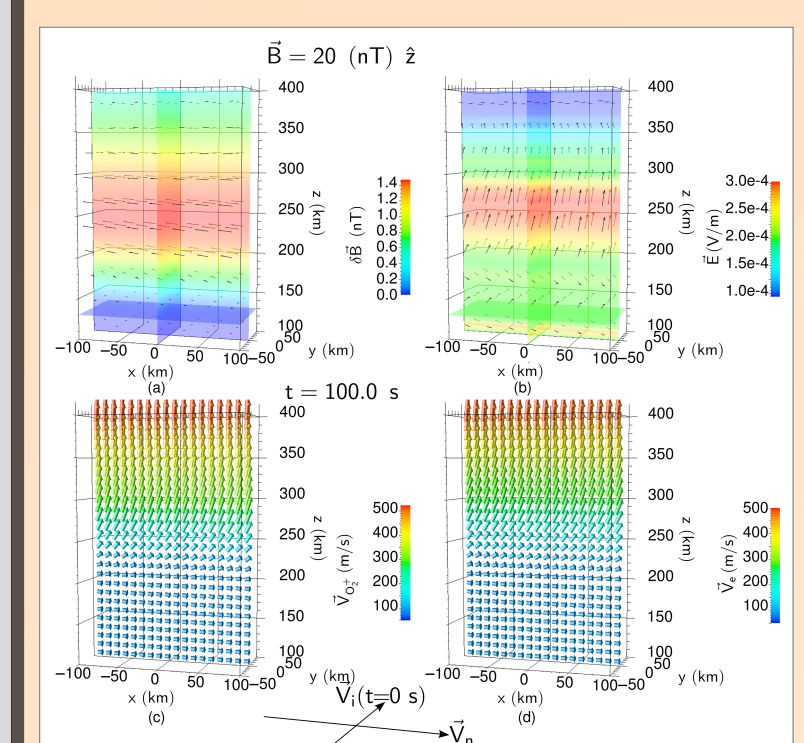

Figure 5: Simulation results at t=100.0 s for $\vec{B}(t{=}0)$=20 nT $\hat{z}$. (a) Magnetic field perturbation $\delta\vec{B}$=$\vec{B}(t)$−$\vec{B}(0)$; (b) Electric field; (c) O_2^+ velocity; (d) electron velocities.

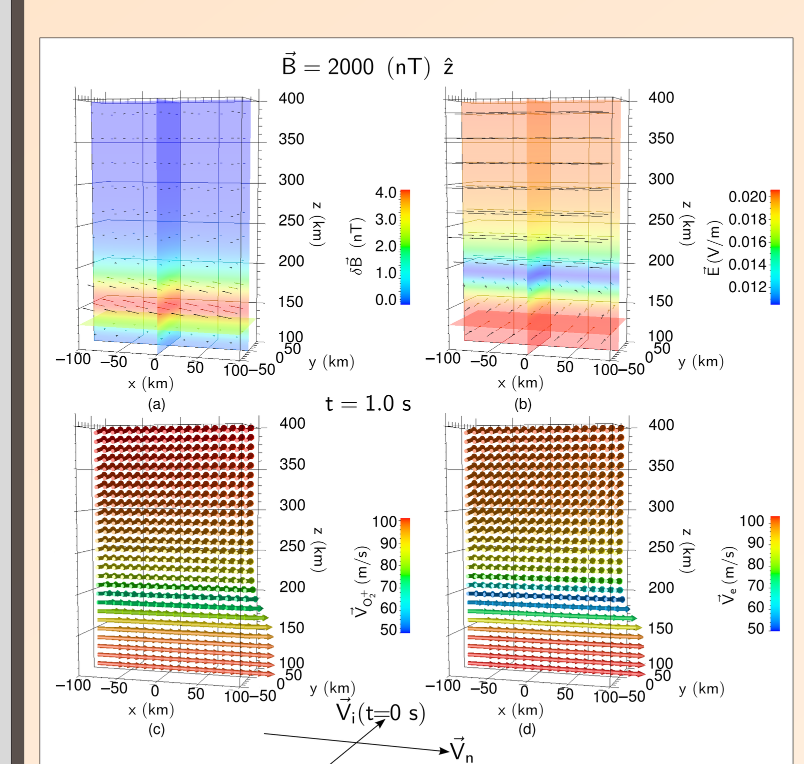

Figure 6: Simulation results at t=1.0 s for $\vec{B}(t{=}0)$=2000 nT $\hat{z}$. (a)–(d) Same as Figure 5.

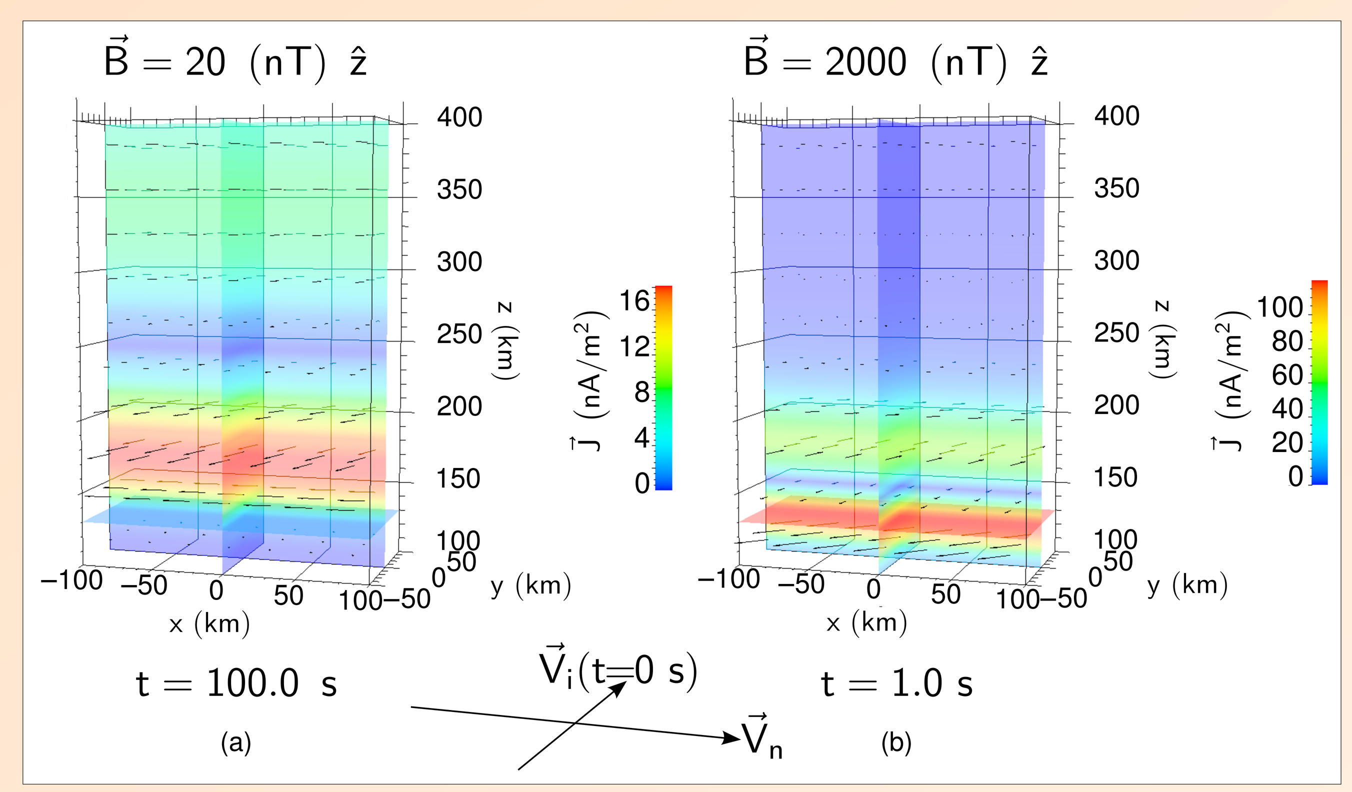

Figure 7: $\vec{J}$ at t=100.0 s for $\vec{B}(t{=}0)$=20 nT $\hat{z}$ (a), and t=1.0 s for $\vec{B}(t{=}0)$=2000 nT $\hat{z}$ (b).

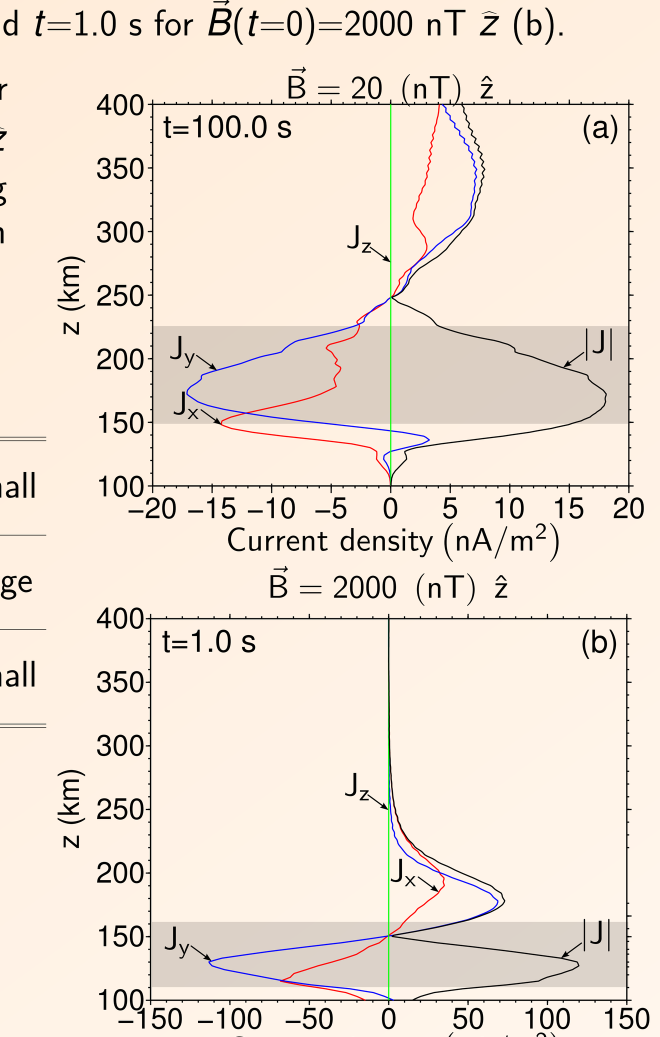

Figure 8: Current density components (J_x, J_y, J_z) at center of the simulation domain at t=100.0 s for $\vec{B}(t{=}0)$=20 nT $\hat{z}$ (a), and t=1.0 s for $\vec{B}(t{=}0)$=2000 nT $\hat{z}$ (b). The gray shading emphasizes the location of the dynamo region expected from Figure 3.

Table 1: Maximum dynamo current

$z \gtrsim H_U$	$\nu_{O_2^+-CO_2} \ll \nu_{c,CO_2}$ $\nu_{e-CO_2} \ll \nu_{c,e}$	Magnetized ions Magnetized electrons	$\vec{J}$ small
$H_L \lesssim z \lesssim H_U$	$\nu_{O_2^+-CO_2} \gtrsim \nu_{c,CO_2}$ $\nu_{e-CO_2} \ll \nu_{c,e}$	Demagnetized ions Magnetized electrons	$\vec{J}$ large
$z \lesssim H_L$	$\nu_{O_2^+-CO_2} \gtrsim \nu_{c,CO_2}$ $\nu_{e-CO_2} \gtrsim \nu_{c,e}$	Demagnetized ions Demagnetized electrons	$\vec{J}$ small

- Between H_U & H_L
- $J_{max} \approx 2e\,n_e\vec{V}_n$
  ↳ $\propto n_e \rightarrow$ Indirect dependence on $\vec{B}$
  ↳ $\propto \vec{V}_n \rightarrow$ Direct dependence on neutral winds

Case 1: $\vec{B}$=20 nT $\hat{z}$
- $n_e \approx 10^4$ cm^{-3}
  ↳ $J_{max} \approx 10^{-7}$ A/m^2

Case 2: $\vec{B}$=2000 nT $\hat{z}$
- $n_e \approx 10^5$ cm^{-3}
  ↳ $J_{max} \approx 10^{-6}$ A/m^2

V. Magnetic Cusps & Loops

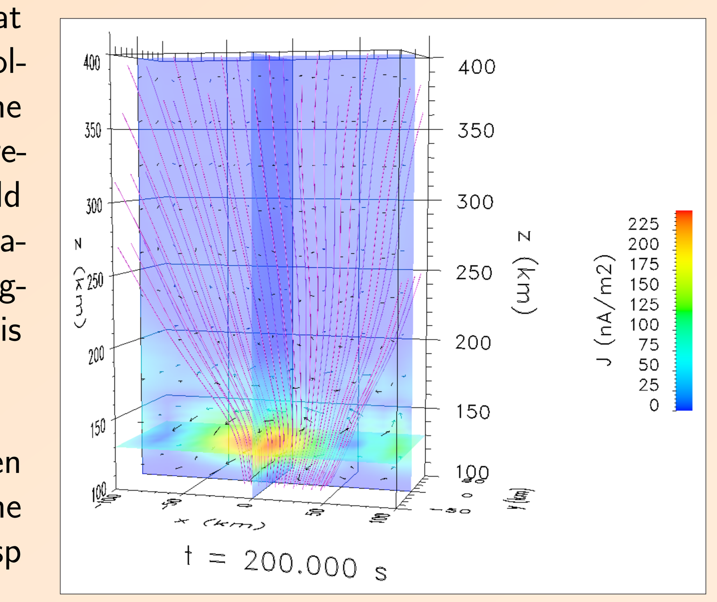

Figure 9: Current densities at t=200.0 s in a cusp region. Colormap and arrows indicate the magnitude and direction of $\vec{J}$, respectively. The magnetic field lines are shown using solid magenta lines. The maximum magnetic perturbation in this case is δB_{max}≈12 nT.

Movie 1: Interactions between the dynamo currents and the crustal magnetic fields in a cusp region as a function of time.

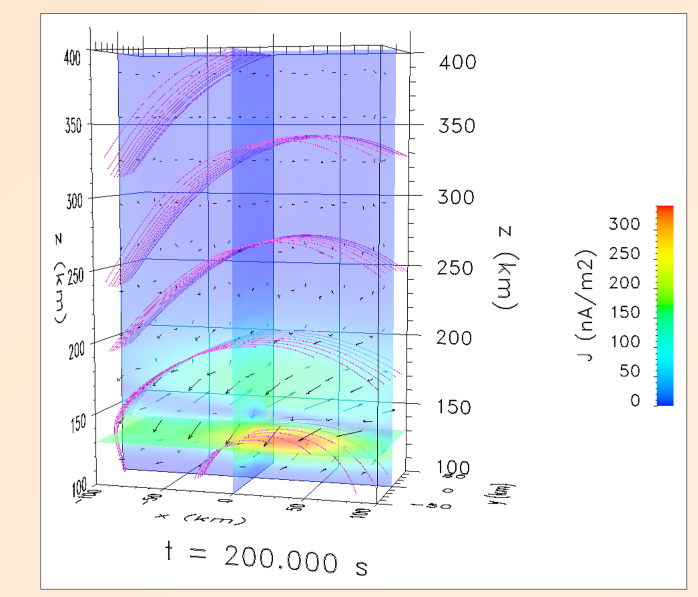

Figure 10: Current densities at t=200.0 s in a loop region. Colormap and arrows indicate the magnitude and direction of $\vec{J}$, respectively. The magnetic field lines are shown using solid magenta lines. The maximum magnetic perturbation in this case is δB_{max}≈25 nT.

Movie 2: Interactions between the dynamo currents and the crustal magnetic fields in a loop region as a function of time.

- $|\vec{B}|$=20 nT @ z=150 km
- $\vec{V}_n$=100 m/s $\hat{x}$
- $\vec{V}_\alpha$=100 m/s $\hat{y}$ @ t=0 s
- $\vec{J}$ develops around 130 km altitude
- $\delta\vec{B}$ appears
- $\vec{B}$-field lines get distorted

VI. Conclusions

The principal results and conclusions developed in this work can be summarized as follows:

- The remanent crustal fields do generate electric currents
- The location of the modeled atmospheric dynamo currents are consistent with those analytically predicted
- The model results for $\vec{J}_{max}$ and $\vec{E}$ are consistent with theoretical calculations
- Mars' ionosphere can be efficiently modeled using a multi-fluid model and therefore our model can be used in more complex geometries
- The 3-D nature of the model is crucial in order to model the structures, currents and fields present in the complex Martian magnetic topology

References

Balay, S., W. D. Gropp, L. C. McInnes, and B. F. Smith (1997), Efficient management of parallelism in object oriented numerical software libraries, in *Modern Software Tools in Scientific Computing*, edited by E. Arge, A. M. Bruaset, and H. P. Langtangen, p. 163–202, Birkhäuser Press.

Brain, D. A., R. J. Lillis, D. L. Mitchell, J. S. Halekas, and R. P. Lin (2007), Electron pitch angle distributions as indicators of magnetic field topology near Mars, *J. Geophys. Res.*, *112*(A9), A09201, doi:10.1029/2007JA012435.

Lewis, S., M. Collins, P. Read, F. Forget, F. Hourdin, R. Fournier, C. Hourdin, O. Talagrand, and J. Huot (1999), A climate database for Mars, *J. Geophys. Res.*, *104*(E10), 24,177–24,194, doi:10.1029/1999JE001024.

Lillis, R. J., D. A. Brain, G. T. Delory, D. L. Mitchell, J. G. Luhmann, and R. P. Lin (2012), Evidence for superthermal secondary electrons produced by SEP ionization in the Martian atmosphere, *J. Geophys. Res.*, *117*(E16), E03004, doi:10.1029/2011JE003932.

Pacheco, P. S. (1996), *Parallel programming with MPI*, Morgan Kaufmann Publishers Inc., San Francisco, CA.

Paty, C., and R. Winglee (2006), The role of ion cyclotron motion at Ganymede: Magnetic field morphology and magnetospheric dynamics, *Geophys. Res. Lett.*, *33*(10), L10106.

Press, W. H., B. P. Flannery, S. A. Teukolsky, and W. T. Vetterling (1992), *Numerical Recipes in C: The Art of Scientific Computing*, 2nd ed., 1020 pp., Cambridge Univ. Press, Cambridge, UK; New York, NY.

This work was supported by the National Aeronautics and Space Administration under grant NNX10AM88G-MFRP to the Georgia Institute of Technology.